

Search for the Decay $\mu^+ \rightarrow e^+ \gamma$

R. D. Bolton, J. D. Bowman, M. D. Cooper, J. S. Frank, A. L. Hallin,^(a) P. A. Heusi,^(b) C. M. Hoffman, G. E. Hogan, F. G. Mariam, H. S. Matis,^(c) R. E. Mischke, D. E. Nagle, L. E. Piilonen, V. D. Sandberg, G. H. Sanders, U. Sennhauser,^(d) R. Werbeck, and R. A. Williams
Los Alamos National Laboratory, Los Alamos, New Mexico 87545

S. L. Wilson,^(e) R. Hofstadter, E. B. Hughes, and M. W. Ritter^(f)
Hansen Laboratories and Department of Physics, Stanford University, Stanford, California 94305

D. Grosnick and S. C. Wright
The University of Chicago, Chicago, Illinois 60637

and

V. L. Highland and J. McDonough
Temple University, Philadelphia, Pennsylvania 19122
 (Received 7 February 1986)

This Letter reports a new experimental search for the family-number–nonconserving decay $\mu^+ \rightarrow e^+ \gamma$. There is no evidence for the presence of this decay mode. The upper limit for the branching ratio is $\Gamma(\mu^+ \rightarrow e^+ \gamma)/\Gamma(\mu^+ \rightarrow e^+ \nu \bar{\nu}) < 4.9 \times 10^{-11}$ (90% confidence limit).

PACS numbers: 13.35.+s, 11.30.Er

No process that violates the conservation of separate lepton numbers¹ has even been observed. Such processes are forbidden in the minimal standard model² of electroweak interactions; their observation would indicate the need for new physics. In many extensions to the standard model,³ decays that do not conserve muon number, such as $\mu^+ \rightarrow e^+ \gamma$, are allowed. The theoretical rates for these processes generally depend upon undetermined parameters such as mixing angles and heavy-particle masses. The existing experimental upper limits for these rates provide model-dependent constraints on these parameters.

The best present experimental upper limit for the branching ratio for $\mu^+ \rightarrow e^+ \gamma$ is⁴

$$B_{\mu e \gamma} = \frac{\Gamma(\mu^+ \rightarrow e^+ \gamma)}{\Gamma(\mu^+ \rightarrow e^+ \nu \bar{\nu})} < 1.7 \times 10^{-10} \text{ (90\% C.L.)}$$

We report here an improved limit for $B_{\mu e \gamma}$ from data taken with the "Crystal Box" detector in the stopped-muon channel at the Clinton P. Anderson Meson Physics Facility (LAMPF). This detector⁵ is designed to identify rare decay modes of the muon. The signature for a $\mu^+ \rightarrow e^+ \gamma$ decay at rest is a positron and a photon with $E_e = E_\gamma = 52.8$ MeV, a time coincidence between the e^+ and the photon, and an opening angle $\theta_{e\gamma}$ between the positron and the photon equal to 180° . The apparatus must be able to measure with precision the energy, direction, and time of emission of photons and positrons to detect the decay $\mu^+ \rightarrow e^+ \gamma$ and to reject backgrounds from muon inner bremsstrahlung ($\mu^+ \rightarrow e^+ \nu \bar{\nu} \gamma$) and random coincidences.

The Crystal Box detector, shown in Fig. 1, consists

of 396 NaI(Tl) crystals, 36 plastic scintillation hodoscope counters, and a cylindrical drift chamber⁶ surrounding a thin polystyrene target in which the muons from a 26-MeV/c beam stop and decay at rest. There is no applied magnetic field. Plastic scintillation veto counters covering the regions upstream and downstream of the hodoscope counters are not shown in the figure. Positron trajectories are measured with the drift chamber. The plastic scintillators are used to distinguish positrons and photons in the trigger and to provide a positron timing signal with a resolution of 290 ps (FWHM). The time of arrival of photons at

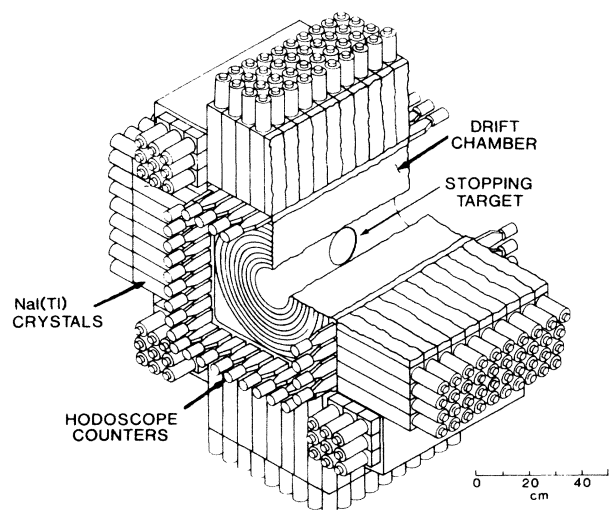


FIG. 1. A schematic diagram of the Crystal Box detector.

the NaI(Tl) is measured with a resolution of 1.2 ns (FWHM). The photon is assumed to originate from the intersection of the positron trajectory with the target plane; the photon conversion point is determined by the distribution of the energy deposition among the NaI(Tl) crystals. The resolution in $\theta_{e\gamma}$ is dominated by the uncertainty in the photon conversion point; the resolution function at 180° can be characterized by a FWHM of 5° . The measured energy resolution at 50 MeV is $\Delta E/E = 8\%$ (FWHM).

Much care was taken to calibrate each of the detector elements and to assure the stability of these calibrations throughout the experiment.⁷ For example, the stability of the energy measurements with the NaI(Tl) array is measured to be constant to better than 0.5% throughout the data and the absolute energy is known to better than 0.25%.

The hardware trigger is based on the four quadrants of NaI(Tl) crystals and hodoscope counters. The requirements for a $\mu^+ \rightarrow e^+\gamma$ candidate are a coincidence within ± 5 ns of a "positron quadrant" and an opposite "photon quadrant." A positron quadrant has a hodoscope counter signal and more than 30 MeV deposited in the NaI(Tl) in that quadrant. A photon quadrant has at least 30 MeV in the NaI(Tl) with no discriminator signal from the hodoscope or veto scintillation counters for that quadrant. The muon stopping rate was typically $4 \times 10^5 \text{ s}^{-1}$ (average) with a duty factor between 5% and 10%. During the course of the experiment, approximately 10^7 triggers were recorded.

The data analysis requires events to satisfy a number of additional criteria designed to eliminate the vast majority of the triggers and to retain for subsequent analysis all good $\mu \rightarrow e^+\gamma$ events and an appreciable sample of inner bremsstrahlung events and random coincidences. Each photon candidate has to deposit less than 0.25 MeV in the 1.27-cm-thick scintillator it traverses and can have no drift-chamber track that points to the photon conversion point in the NaI(Tl). There can be no scintillator discriminator signal other than the one in the positron quadrant. The e^+ candidate has to have a track in the drift chamber with a trajectory that intersects the target plane with an angle greater than 3° . A restricted data sample of 17 073 events satisfies $|\Delta t_{e\gamma}| < 5$ ns, $\theta_{e\gamma} > 160^\circ$, $E_e > 44$ MeV, and $E_\gamma > 40$ MeV.

Figure 2(a) shows $\Delta t_{e\gamma}$, the photon-positron relative timing, for a subset of these events. This figure shows the broad timing distribution due to random photon-positron triggers and a coincidence peak; the width of this peak is 1.2 ns (FWHM). The majority of the events in the coincidence peak are due to muon inner bremsstrahlung but any $\mu \rightarrow e\gamma$ events would also be included. It is the task of the subsequent analysis to determine how many of these events are due to μ

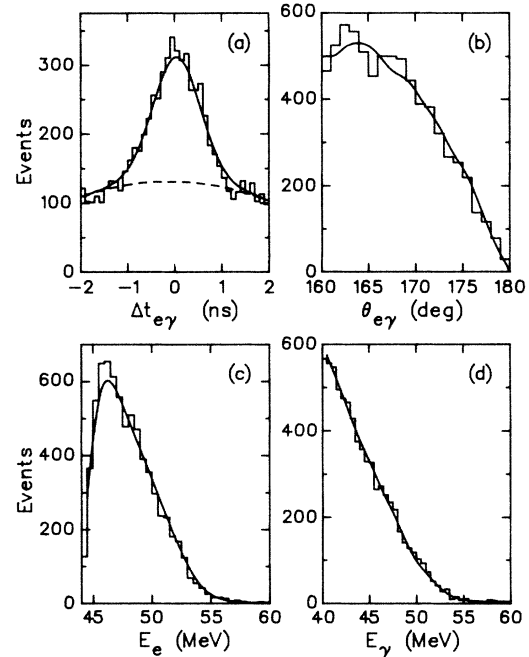


FIG. 2. Spectra from 68% of the data sample for each of the quantities used in the likelihood analysis. (a) The distribution of $\Delta t_{e\gamma}$, the relative timing between the positron and the photon. The solid curve is the fit to these data with a Gaussian for $\mu \rightarrow e\gamma\nu\nu$ plus a quadratic for randoms. The dashed curve is the random background in the fit. (b)–(d) The distributions of $\theta_{e\gamma}$, E_e , and E_γ . The curves are the sum of Monte Carlo spectra for $\mu \rightarrow e\gamma\nu\nu$ and random spectra obtained from out-of-time events.

$\rightarrow e\gamma$. The kinematic quantity $E + P = E_e + E_\gamma + |\mathbf{P}_e + \mathbf{P}_\gamma|$ is used to select events due to random triggers; events with $E + P > M_\mu$ cannot come from a positron and a photon emerging from a single muon decay. The dashed curve in Fig. 2(a) comes from a quadratic fit to the random background and a Gaussian line shape for the coincidence events, but it is also a good representation of $\Delta t_{e\gamma}$ for events with $E + P > 115$ MeV. The curve is rounded by the differing losses of efficiency for the many detector elements in the coincidence logic for large $|\Delta t_{e\gamma}|$.

To estimate the number of $\mu \rightarrow e\gamma$ events in the data sample we employ the maximum-likelihood method. The likelihood function is defined to be⁴

$$L(N_{e\gamma}, N_{IB}) = \prod_{i=1}^N \left[\frac{N_{e\gamma}}{N} P(\mathbf{x}_i) + \frac{N_{IB}}{N} Q(\mathbf{x}_i) + \frac{N_R}{N} R(\mathbf{x}_i) \right],$$

where N is the total number of events, $N_{e\gamma}$ (N_{IB}) is the estimate of the number of $\mu \rightarrow e\gamma$ ($\mu \rightarrow e\gamma\nu\nu$) events, and $N_R = N - N_{e\gamma} - N_{IB}$ is the number of events due to random backgrounds. The vector \mathbf{x} has components $\theta_{e\gamma}$, $\Delta t_{e\gamma}$, E_e , and E_γ . P , Q , and R are the

normalized probability distributions for $\mu \rightarrow e\gamma$, inner bremsstrahlung, and random background events, respectively. The best estimates for $N_{e\gamma}$ and N_{IB} are those that maximize the likelihood function for positive $N_{e\gamma}$ and N_{IB} .

The $\Delta t_{e\gamma}$ behavior of each distribution is obtained as described above. A Monte Carlo program is used to determine the dependence of P and Q on $\theta_{e\gamma}$, E_e , and E_γ . Out-of-time data events give the R probability distributions for $\theta_{e\gamma}$, E_e , and E_γ . The Monte Carlo program accurately reproduces the response of the detectors to positrons and photons. Electromagnetic showers are simulated with the shower code EGS3.⁸ The output events from the Monte Carlo program are processed by the same programs as the data with use of the same algorithms for the NaI(Tl) energy and position determination. While the $\Delta t_{e\gamma}$ dependences of P and Q are the same, the other distributions are markedly different; these differences allow the maximum-likelihood method to determine separately the number of muon inner-bremsstrahlung and $\mu \rightarrow e\gamma$ events.

Figure 3 shows the normalized likelihood function. The function peaks at $N_{IB} = 3470 \pm 80$ and $N_{e\gamma} = 0$. There is an additional uncertainty in N_{IB} of ± 300 due to uncertainties in the shape of the random timing distribution under the coincidence peak; this uncertainty does not affect $N_{e\gamma}$. N_{IB} agrees reasonably well with the 3960 ± 90 inner-bremsstrahlung events expected in the data. The number of inner-bremsstrahlung events is very sensitive to the absolute energy measurement scale; a 2% change in the NaI(Tl) gain would imply a factor of 2 change in the expected number of muon inner-bremsstrahlung events. The agreement also ver-

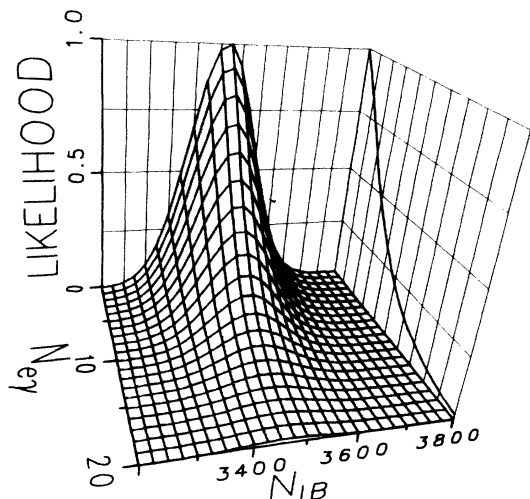


FIG. 3. The normalized likelihood function plotted as a function of the number of inner-bremsstrahlung events and the number of $\mu \rightarrow e\gamma$ events. The projected distribution on the $N_{e\gamma}$ -likelihood plane is also shown.

ifies our understanding of the muon flux, the acceptance and detection efficiency of the apparatus and the shapes of the probability distributions.

The likelihood-function distribution implies $N_{e\gamma} \leq 11$ events (90% C.L.). Using the number of muons stopped in the target during the live time of the experiment (1.35×10^{12}), the apparatus acceptance for $\mu \rightarrow e\gamma$ (0.305), and the detection efficiency (0.545), we obtain

$$B_{\mu e\gamma} < 4.9 \times 10^{-11} \text{ (90\% C.L.)}.$$

We have subjected the data to a number of systematic checks. The measured opening-angle and energy spectra for the in-time and random events agree with the Monte Carlo spectra. The agreement is demonstrated in Figs. 2(b)–2(d) where the spectra for $\theta_{e\gamma}$, E_e , and E_γ for the data are compared to the spectra for the appropriate sum of random events and Monte Carlo simulations of $\mu \rightarrow e\gamma\nu\nu$. The normalizations for the latter spectra are taken from the maximum-likelihood fit. Consistent results are obtained for each of several data subsets including data with the positron in a particular quadrant, data taken with different instantaneous muon stopping rates, and data taken early or late in the run.

As examples of theoretical constraints imposed by our result, we show how this new value of $B_{\mu e\gamma}$ limits the parameters in a complete model and in supersymmetric theories. With use of the formula of Tomozawa⁹ for the mass of the constituents of muons and electrons, where the muon is taken to be a $2S$ excited state of the electron, $B_{\mu e\gamma}$ can be combined with $B_{\mu e\gamma\gamma}$ ¹⁰ to yield a lower limit on the mass of the constituents of 5.8×10^8 GeV. In broken supersymmetric theories,¹¹ where the symmetry is broken by gravity,¹² the mass of the supersymmetric partner of the muon must be greater than 36 GeV. In both cases, the mass limits vary as $[B_{\mu e\gamma}]^{-1/4}$.

In summary, we see no evidence for the family-nonconserving decay $\mu \rightarrow e\gamma$ at a level of 4.9×10^{-11} (90% C.L.). The upper limit for the branching ratio for this decay has improved nearly 3 orders of magnitude since the advent of "meson factories." We expect a further improvement in the sensitivity by a factor of 500 in an upcoming experiment.¹³

There are a great many people who contributed in a major way to the success of this experiment. It is impossible to list them individually here but we do want to acknowledge the extraordinary assistance we had from many people at each of our institutions and from the operations staff at LAMPF. This work was supported in part by the U.S. Department of Energy and the National Science Foundation.

(a)Present address: Physics Department, Princeton University, Princeton, N.J. 08544.

^(b)Present address: ELEKTROWATT Ing. AG., Zurich, Switzerland.

^(c)Present address: Lawrence Berkeley Laboratory, Berkeley, Cal. 94720.

^(d)Present address: Swiss Institute for Nuclear Research, CH-5234 Villigen, Switzerland.

^(e)Present address: Los Alamos National Laboratory, Los Alamos, N. Mex. 87545.

^(f)Present address: Lockheed Missiles and Space Company, Palo Alto, Cal. 94304.

¹J. Schwinger, *Ann. Phys. (N.Y.)* **2**, 407 (1957); K. Nishijima, *Phys. Rev.* **108**, 907 (1957); S. Bludman, *Nuovo Cimento* **15**, 173 (1958).

²S. L. Glashow, *Nucl. Phys.* **22**, 579 (1961); A. Salam, in *Elementary Particle Theory: Relativistic Groups and Analyticity*, Nobel Symposium No. 8, edited by N. Svartholm (Almqvist and Wiksells, Stockholm, 1968), p. 367; S. Weinberg, *Phys. Rev. Lett.* **19**, 1264 (1967).

³A brief discussion of many of these extensions can be found in C. M. Hoffman, in *Fundamental Interactions in Low-Energy Systems*, edited by P. Dalpiaz, G. Fiorentini, and

G. Torelli (Plenum, New York, 1985), p. 138; P. Herczeg and T. Oka, *Phys. Rev. D* **29**, 475 (1984); D. E. Nagle, *Comments Nucl. Part. Phys.* **11**, 277 (1983).

⁴W. W. Kinnison *et al.*, *Phys. Rev. D* **25**, 2846 (1982).

⁵See R. D. Bolton *et al.*, *Phys. Rev. Lett.* **53**, 1415 (1984), and references therein.

⁶R. D. Bolton *et al.*, *Nucl. Instrum. Methods* **241**, 52 (1985).

⁷S. L. Wilson, Ph.D. thesis, Stanford University, Los Alamos National Laboratory Report LA-10471-T, 1985 (to be published).

⁸R. L. Ford and W. R. Nelson, Stanford Linear Accelerator Center Report No. SLAC 210, 1978 (unpublished).

⁹Y. Tomozawa, *Phys. Rev. D* **25**, 1488 (1982).

¹⁰D. P. Grosnick *et al.*, in *Proceedings of the Santa Fe Meeting*, edited by T. Goldman and M. M. Nieto (World Scientific, Singapore, 1985), p. 237.

¹¹J. Ellis and D. V. Nanopoulos, *Phys. Lett.* **110B**, 41 (1983).

¹²E. Cremmer *et al.*, *Phys. Lett.* **122B**, 41 (1983).

¹³M. D. Cooper *et al.*, unpublished.